A *Chandra* observation of the X-ray environment and jet of 3C 296

M.J. Hardcastle[1,2], D.M. Worrall[2], M. Birkinshaw[2], R.A. Laing[3,4] and A.H. Bridle[5]

[1] *School of Physics, Astronomy and Mathematics, University of Hertfordshire, College Lane, Hatfield, Hertfordshire AL10 9AB*
[2] *Department of Physics, University of Bristol, Tyndall Avenue, Bristol BS8 1TL*
[3] *European Southern Observatory, Karl-Schwarzschild-Strasse 2, D-85748 Garching-bei-München, Germany*
[4] *University of Oxford, Department of Astrophysics, Denys Wilkinson Building, Keble Road, Oxford OX1 3RH*
[5] *National Radio Astronomy Observatory, 520 Edgemont Road, Charlottesville, VA 22903-2475, U.S.A*

1 August 2007

ABSTRACT

We have observed the twin-jet radio galaxy 3C 296 with *Chandra*. X-ray emission is detected from the nucleus, from the inner parts of the radio jet, and from a small-scale thermal environment around the jet deceleration region. As we have found in previous observations of other twin-jet radio galaxies, the X-ray jet and a steep pressure gradient in the external thermal environment are associated with the region where strong bulk deceleration of the jet material is suggested by radio observations. Our observations provide additional evidence that the inner jets of twin-jet objects are always associated with a relatively cool, dense central X-ray emitting component with a short cooling time.

Key words: galaxies: active – X-rays: galaxies – galaxies: individual: 3C 296 – galaxies: jets – radiation mechanisms: non-thermal

1 INTRODUCTION

In an earlier paper (Hardcastle et al. 2002) we reported on *Chandra* X-ray observations of the twin-jet FRI radio galaxy 3C 31. It has been accepted for some time that the jets in this class of radio galaxy often have relativistic bulk speeds on parsec scales but transsonic or sub-sonic speeds on scales of hundreds of kiloparsecs, so that they must decelerate on intermediate scales. The available observational evidence from studies of large samples and of individual objects (e.g. Laing et al. 1999; Laing & Bridle 2002a) suggests that this deceleration happens on scales of $\sim$ 1–10 kpc for FRIs of intermediate to high power, corresponding to scales of a few arcseconds at the 100-Mpc distances of typical well-studied objects. It is thus possible to study the deceleration region with *Chandra* and the NRAO Very Large Array (VLA).

Combined X-ray and radio observations of the jet deceleration regions are important for two reasons. Firstly, all models in which the jet decelerates by mass loading require an external pressure gradient to prevent the jet from decollimating and disrupting. The hot, X-ray emitting phase of the ISM/IGM is the only one with sufficient pressure to be dynamically important in this situation. By observing the X-ray emitting medium on scales of a few kpc we can test the jet deceleration model both qualitatively (the steep pressure gradient must be detected for standard models to operate) and quantitatively (by comparing with the observations predictions of the external pressure based on detailed modelling of the radio emission). Secondly, the internal dissipation of energy that arises from bulk deceleration can help to explain the X-ray synchrotron jets seen in the inner few kpc of many twin-jet FRIs (e.g. Worrall et al. 2001, 2003; Hardcastle et al. 2001). The X-ray jet emission

may itself be an indication of bulk deceleration, and there is some direct evidence for this in the dynamics of the nearest such jet, Cen A (Hardcastle et al. 2003).

In our *Chandra* observations of 3C 31 we detected both an X-ray synchrotron jet and a kpc-scale thermal environment with a steep pressure gradient. Subsequently it was possible to show (Laing & Bridle 2002b) that the form of the external pressure profile was similar to that predicted from detailed modelling of the radio jet properties (Laing & Bridle 2002a), and to derive good constraints on the kinetic luminosity of the jet. The brightest X-ray emission occurs in the region of the jet immediately before the rapid deceleration inferred from radio modelling. These observations of 3C 31 provided strong support for the jet deceleration model, but it is important to explore whether this model applies to other objects. We report here on the result of our *Chandra* observations of 3C 296, which is another twin-jet radio galaxy suitable for modelling in this way.

3C 296 is a well-known FRI radio source (Birkinshaw, Laing & Peacock 1981; Leahy & Perley 1991; Hardcastle et al. 1997) hosted by the elliptical galaxy NGC 5532 at a redshift of 0.0237, a similar redshift to that of NGC 383 which contains 3C 31. Like NGC 383, NGC 5532 lies in a group of galaxies, including at least one bright nearby galaxy, NGC 5531; the association of the group galaxies has been confirmed spectroscopically (Miller et al. 2002). In the X-ray, 3C 296 was detected with *Einstein* (Fabbiano et al. 1984), the *ROSAT* HRI (Hardcastle & Worrall 1999) and the *ROSAT* PSPC (Miller et al. 1999). Radio sidedness studies (Hardcastle et al. 1997) suggest that the jet decelerates significantly on

scales of about 10 arcsec, making it a good candidate for *Chandra* observations.

Throughout the paper we use a concordance cosmology with $H_0 = 70$ km s^{-1} Mpc^{-1}, $\Omega_m = 0.3$ and $\Omega_\Lambda = 0.7$. At the redshift of 3C 296, 1 arcsec corresponds to 480 pc. Spectral indices α are the energy indices and are defined in the sense $S_\nu \propto \nu^{-\alpha}$. The photon index Γ is $1 + \alpha$.

2 THE OBSERVATIONS

3C 296 was observed for 49429 s with the *Chandra* ACIS-S on 2003 August 31. The source was positioned near the standard aim point on the back-illuminated S3 CCD. We reprocessed the data in the standard way to apply the latest calibration files (using CIAO 3.1 and CALDB 2.28). As the data were taken in VFAINT mode, we used 'VFAINT cleaning' to identify and reject some background events. We also removed the 0.5-pixel event position randomization and removed streaking from the S4 chip.

We used events in the energy range 0.5–5 keV to construct an image (throughout the paper this energy range is used for imaging). As Fig. 1 shows, there is a clear detection of an X-ray core and jet, as well as extended emission extending out to scales of tens of arcsec. In addition, on larger scales, X-ray emission is detected from the nearby galaxy seen in *HST* images (Martel et al. 1999 class it as an S0) and from NGC 5531. The spatial and spectral properties of these components are discussed in the following sections. Spectra were extracted and corresponding response matrices constructed using CIAO, and model fitting was carried out (in the energy range 0.4-7.0 keV) in XSPEC. In all cases, except where otherwise stated, the extracted spectra were grouped so that each fitting bin had > 20 counts after background subtraction. Errors quoted throughout are the 1σ value for one interesting parameter, unless otherwise stated.

3 THE X-RAY CORE

As we will show in Section 6, the thermal emission from the host galaxy of 3C 296 has a small angular scale. It is therefore not possible spatially to isolate the X-ray nucleus completely. We extracted a spectrum from an circle of radius 1.5 arcsec, taking background from an annulus between 1.5 and 2.5 arcsec. These small regions were intended to minimize the contribution from thermal emission and also avoid the nearby point source and resolved jet. There are 914 net counts in the 0.4–7.0 keV energy range in this region. Unsurprisingly, the resulting spectrum is not well fitted ($\chi^2 = 66.3$ for 38 degrees of freedom) by a single power-law model with Galactic absorption ($N_H = 1.85 \times 10^{20}$ cm^{-2}) and shows large residuals at around 1 keV. The fit is unimproved if the absorbing column is allowed to vary. A combination of a power law and a MEKAL model with 0.5 solar abundance, both with Galactic absorption, is a better fit ($\chi^2 = 41.4$ for 36 d.o.f.) but gives an unusually flat photon index, $\Gamma = 0.77^{+0.09}_{-0.08}$; the temperature of the thermal component in this model is 0.61 ± 0.07 keV. The best fits ($\chi^2 = 27.6$ for 35 d.o.f.) are obtained if we allow the power-law model to be intrinsically absorbed: in this case the intrinsic column is $(1.0 \pm 0.5) \times 10^{22}$ cm^{-2}, the photon index is 1.6 ± 0.4 (the errors for these two quantities are 1σ for two interesting parameters, as they are correlated), and the MEKAL model has $kT = 0.62 \pm 0.05$ keV. In this model, almost all the counts below 1 keV are contributed by the thermal component, and this interpretation is supported by imaging, which shows the source to be much more point-like above 1 keV than below it.

The power-law component would contribute 530^{+240}_{-160} counts to our extraction region in this model, or roughly half of the total, and its normalization corresponds to an unabsorbed 1-keV flux density of 24 nJy; its absorbed 2–10 keV flux is 1.7×10^{-13} ergs cm^{-2} s^{-1}. No additional component (e.g. a second unabsorbed power law) gives a significant improvement over this fit.

Intrinsic obscuration with large columns is rare, but not unknown, in FRI sources (e.g. Hardcastle et al. 2002; Donato, Sambruna & Gliozzi 2004; Evans et al. in prep.). The inferred column density for 3C 296 is among the largest yet reported for an FRI, comparable to that seen in 3C 270 (Gliozzi, Sambruna & Brandt 2003). It is noteworthy that the two FRI sources known to have high X-ray absorption columns, 3C 270 and 3C 296, also both show an unresolved nuclear component in the optical but not the UV (Chiaberge et al. 2002); this is possible evidence that the optical and X-ray emission in these sources originate on the same spatial scales.

Although large for an FRI source, the column density seen in 3C 296 is much less than the columns of a few $\times 10^{23}$ cm^{-2} inferred for obscuring 'tori' in FRI sources like Centaurus A (e.g. Evans et al. 2004) or FRIIs like Cygnus A (Ueno et al. 1994). As we have pointed out previously (e.g. Hardcastle et al. 2002) the presence or absence of a moderate absorbing column (which could be related to the known presence of cold, dusty gas in the centres of these galaxies) in the nuclear X-ray emission does not provide any direct information on the presence or absence of an obscuring torus around the central AGN if the X-ray emission is jet-dominated and originates on scales larger than that of the AGN; in this scenario we would see evidence for a torus only in sources with very weak jets (Cen A) or very strong AGN (Cyg A). We will return to this point elsewhere (Evans et al. in prep.).

Small-scale thermal emission is common in fits to cores of these systems, and we will discuss this component further in Section 6. The abundance of the thermal component is not well constrained if we allow it to be a free parameter, since the absorption column and normalization of the power-law component of the fit can be adjusted to allow for any value of the ratio between the line emission and continuum emission in the MEKAL model. Our choice to fix the value to 0.5 solar is consistent with Section 6.

4 THE X-RAY JET

X-ray emission is detected from the northern jet, starting at around 2 arcsec from the nucleus and extending to about 10 arcsec. The spatial scale corresponds closely to the bright inner region of the radio jet (Fig. 1), immediately before the location where the radio sidedness data imply a sudden deceleration (Hardcastle et al. 1997). We extracted a spectrum in a rectangular region 7.1 arcsec long and 2.6 arcsec wide, aligned with the jet and starting at 2 arcsec from the nucleus. There are 74 net counts in the 0.4–7.0 keV energy range, after subtracting background from an identical region at a different position angle with respect to the nucleus (this background subtraction procedure was chosen to ensure subtraction of the correct level of background due to the extended thermal emission discussed in Section 6). We binned the extracted spectrum with 18 counts per spectral bin to avoid discarding data. The spectrum is well fitted ($\chi^2 = 1.4$ for 2 d.o.f.) with a single power law with Galactic absorption: the spectral index α is 1.0 ± 0.4 and the normalization corresponds to an unabsorbed 1-keV flux density of 1.2 ± 0.3 nJy. This makes the jet substantially fainter (both in terms of X-ray flux density and X-ray luminosity) than those seen
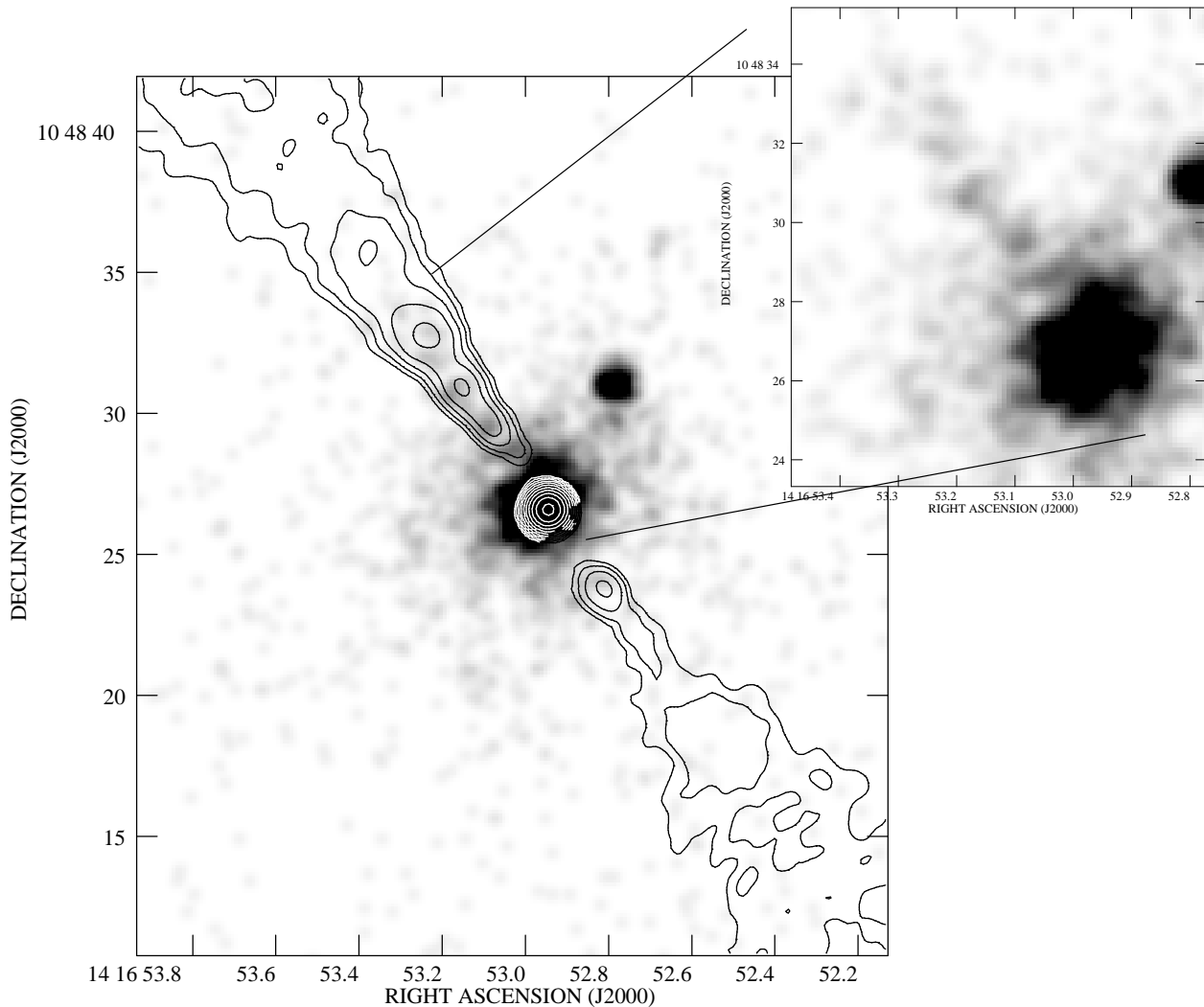
Figure 1. *Chandra* image of the inner regions of 3C 296. The greyscale is the X-ray data binned in 0.123-arcsec pixels and smoothed with an 0.5-arcsec (FWHM) Gaussian: black is 1 count pixel^{-1}. Superposed are contours from the 8.4-GHz, 0.75-arcsec resolution radio map obtained with the VLA by Hardcastle et al. (1997); the contours are drawn at $100 \times (1, 2, 4, \ldots)$ μJy beam^{-1}. The X-ray point source to the NE is discussed in section 5.1. The inset shows the inner part of the jet without radio contours, but with the same greyscale level.

in some other 3CRR FRI sources, though the X-ray spectral index is similar.

The 8.4-GHz flux density in the same region is 17.5 mJy, so that the two-point radio-to-X-ray spectral index is 0.96 ± 0.01, somewhat steeper than is seen in other 3CRR sources (the median value for known jets is 0.92), but comparable to the extended emission in Cen A (Hardcastle et al. 2003). Since the radio spectral index in the inner jets is 0.6 (Hardcastle et al. 1997) fitting the now standard synchrotron model to the radio and X-ray data points requires a break in the synchrotron spectrum; locating the break requires constraints from optical observations. There is no evidence for an optical jet in the *Hubble Space Telescope* Wide Field/Planetary Camera 2 image taken in the F702W filter (Martel et al. 1999) after subtraction of a model of the elliptical isophotes: based on the level of structure in the residual image, we place a limit on the jet flux density at 4.34×10^{14} Hz of $\lesssim 10$ μJy. Similarly, we were unable to detect jet emission in ground-based optical images. However, there is a weak jet detection in the *HST* STIS image centred around 2200 Å and taken in 2000 (Allen et al. 2002),

extending out to the edge of the STIS field of view, 8.5 arcsec from the core. An image of this jet detection is shown in Fig. 2. After background subtraction, correction for the relative sizes of the STIS and *Chandra* extraction regions and scaling for an estimated 0.25 mag of Galactic extinction at 2200 Å, we estimate a flux density at 1.3×10^{15} Hz for the jet region of 1.9 μJy. This allows us to construct a spectrum for the jet that is similar to those of other sources (Fig. 3).

As with other jets of this kind, the inverse-Compton emission mechanism (assuming no beaming and only synchrotron and CMB photons as the parent photon population) underpredicts the observed X-ray by several orders of magnitude (the predicted spectra are plotted on Fig. 3) unless there is a large departure from the equipartition/minimum-energy conditions. We conclude that the jet is another example of the association between X-ray synchrotron radiation and the inner, dissipative jet of an FRI source. There is some evidence that the X-ray-to-radio flux density ratio falls with distance along the jet, as seen in other jets: the ratio of 1-keV to 8.4-GHz flux densities between 2 and 4 arcsec from the
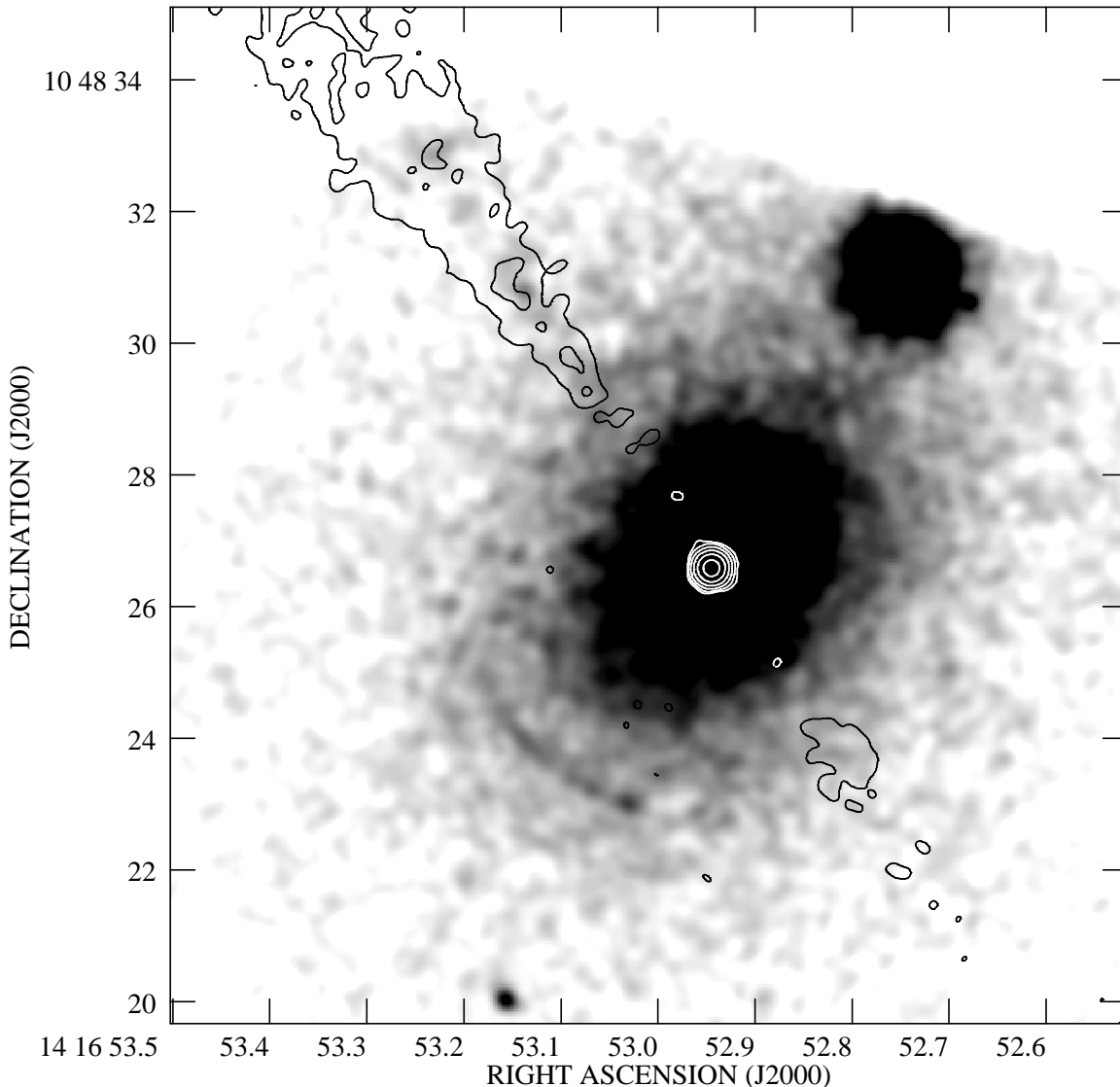
Figure 2. The *HST* STIS image of 3C 296 at 2200 Å, convolved with a 0.25-arcsec (FWHM) circular Gaussian. Overlaid are contours of the 0.24-arcsec resolution 8.4-GHz radio map of Hardcastle et al. (1997) at $60 \times (1, 4, 16...) \mu$Jy beam^{-1}. There is a weak but significant excess of emission in the position angle of the jet. The bright source to the NW is the optical counterpart of the X-ray point source in Fig. 1, and is discussed in Section 5.1. The arc-like feature SW of the core is discussed in Section 5.4.

core is $(0.14 \pm 0.05) \times 10^{-6}$, while between 4 and 10 arcsec it is $(0.05 \pm 0.01) \times 10^{-6}$.

No X-ray emission is detected from the counterjet of 3C 296. The radio flux density in the equivalent region of the counterjet is around 6 mJy, so naively we might expect to see around 1/3 of the jet counts, or 25 in total, from the counterjet region. If the jet sidedness is due entirely to beaming, then (as we pointed out in the case of 3C 31) the expected jet-counterjet ratio in the X-ray is greater than that in the radio, as a result of the steeper X-ray spectral index, and in fact we would expect about 20 counts in total. As the 1σ uncertainty in the number of counts in the counterjet region is around 10, we cannot rule out the possibility that the counterjet really is emitting X-rays at the predicted level. The same comment applies to the brightest region of the counterjet, the knot at 3 arcsec from the core, where the upper limits are insufficient to rule out the possibility that this component is emitting at its expected level of

~ 7 counts. We therefore cannot say with these data whether the jet and counterjet have identical spectra over the radio to X-ray range.

5 NEARBY AND ASSOCIATED OBJECTS

5.1 The nearby point source

The X-ray source 5 arcsec to the NW of 3C 296's core is associated with bright UV emission (Fig. 2) and weak optical emission (Fig. 4). In the X-ray its radial profile is consistent with that of a point source, and its optical counterpart is also point-like. It contains 135 net *Chandra* counts in a 1.2-arcsec source circle, with background taken from a concentric annulus between 1.2 and 1.7 arcsec, and is well fitted ($\chi^2 = 6.0$ for 4 degrees of freedom) with a power law with Galactic absorption, but with a remarkably steep spectrum, $\Gamma = 4.4 \pm 0.4$. (A black-body model with $kT \sim 0.1$
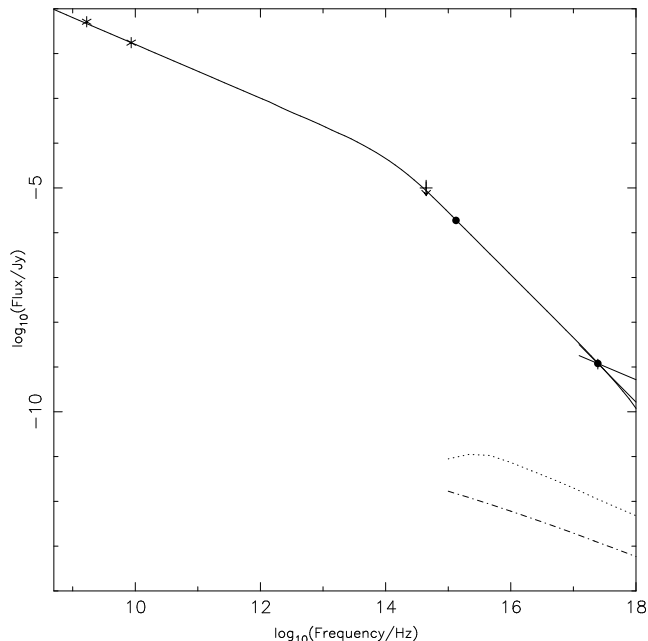
Figure 3. The radio-to-X-ray spectrum of the jet of 3C 296, based on the region detected with *Chandra*. Radio points (stars) are taken from the data of Hardcastle et al. (1997); the optical data points are from archival *HST* data, as described in the text. The 'bow tie' around the X-ray flux density illustrates the 1σ range of spectral index in the power-law fit to the jet spectrum. The solid line shows a broken power-law synchrotron model, with low-frequency spectral index 0.55 and high-frequency spectral index 1.4. The dotted and dash-dotted lines show the predicted X-ray emission for inverse-Compton scattering of the cosmic microwave background and for the synchrotron self-Compton process respectively, assuming minimum-energy conditions.

keV is an unacceptably poor fit, $\chi^2 = 9$ for 4 d.o.f.) Its 1-keV flux density on the power-law model is 17.8 nJy. Re-examination of the *ROSAT* HRI data shows a weak elongation of the X-rays in the direction of this point source, consistent with the idea that it was present at that epoch, although the significance of the elongation is limited in view of the known problems with *ROSAT* aspect reconstruction. There is no evidence for inter-observation variability in the *Chandra* data. The optical counterpart is only weakly detected in the F702W WFPC2 *HST* image taken in 1994 and shown in Fig. 4 (flux density at 4.3×10^{14} Hz is 2.3 μJy: $R \sim 23$ mag), but more strongly in an ACS HRC F606W image taken in 2002 (47 μJy at 5.1×10^{14} Hz) and is very strong in the STIS image discussed above (93 μJy at 1.3×10^{15} Hz). If taken at face value (neglecting any possible optical variability of the source) then the object's broad-band spectrum would be strongly peaked in the UV.

The object's very faint optical magnitude means that it is difficult to associate it with any Galactic source, particularly given the high Galactic latitude ($64°$) of 3C 296. A hot white dwarf in the Galactic halo would be one possible identification: the X-ray luminosity is in the observed range, but the extreme optical colour (or optical variability) argues against such a model. If the X-ray source were actually at the distance of NGC 5532, its unabsorbed X-ray flux in the *ROSAT* band (0.1–2.4 keV) of 4.8×10^{-13} ergs cm^{-2} s^{-1} would give it a luminosity in this band of 6×10^{41} ergs s^{-1}, which would make it extreme even for an ultra-luminous X-ray source; in particular, it would be $\sim$ 1.5–2 orders of magnitude more luminous than ultra-luminous supersoft sources such as the one in M101 (Mukai et al. 2003). We therefore conclude that it is

most likely to be a spectrally peculiar background AGN, possibly amplified in brightness to some extent by lensing (see Section 5.4).

5.2 The nearby spiral

As Fig. 4 shows, the X-ray emission from this galaxy (which, from its magnitude, is likely to be a member of the NGC 5532 group, although it has not been spectroscopically confirmed to be one) is mostly associated with the galactic plane, but there is a weak but significant detection of emission further away from it. There are insufficient counts from this region to fit a spectrum to the two components separately. The 60 net counts in the combination of the two are well fitted ($\chi^2 = 0.60$ for 1 degree of freedom) with a power-law model with Galactic absorption and a flat spectrum ($\Gamma = 1.2 \pm 0.3$). The unabsorbed 2–10 keV flux of the galaxy is 1.3×10^{-14} ergs cm^{-2} s^{-1}, corresponding to a luminosity of 1.7×10^{40} ergs s^{-1} in this band if the galaxy is at the distance of NGC 5532. This is a plausible luminosity for a large spiral galaxy.

5.3 NGC 5531

Both extended and compact emission is detected from the nearby elliptical galaxy NGC 5531. In a source circle 30 arcsec in size (taking background from a concentric annulus between 30 and 40 arcsec) there are 270 net counts in the 0.4–7.0 keV energy band. Fitting with a single power-law model with Galactic absorption gives a poor fit ($\chi^2 = 17.4$ for 10 d.o.f.), with residuals below 1 keV, and fitting a thermal model alone gives an even worse fit; a better fit is given by fitting a combination of a power-law model and a thermal (MEKAL) component with fixed 0.3 solar abundances ($\chi^2 = 10.8$ for 8 d.o.f.: $kT = 0.44 \pm 0.10$ keV, $\Gamma = 2.2^{+0.4}_{-0.7}$). This, together with the images, suggests that there is some harder nuclear X-ray emission from NGC 5531, together with extended thermal emission. The unabsorbed 2–10 keV flux of the galaxy is 1×10^{-14} ergs cm^{-2} s^{-1}, almost all provided by the power-law component, or 1.3×10^{40} ergs s^{-1}: given that NGC 5531 is around 1.5 magnitudes fainter than NGC 5532 in the optical, we cannot rule out the possibility that all the hard X-ray emission comes from a population of X-ray binaries (see Section 6).

5.4 The ultraviolet arc SE of NGC 5532.

The ultraviolet feature evident about 2 arcsec (1 kpc) SE of the centre of NGC 5532 (Fig. 2) has the appearance of a gravitationally-lensed arc. Such features are now relatively common in clusters of galaxies (for example in Abell 370; Lynds & Petrosian 1989), but more usually only point-like lenses are seen near galaxies (e.g., from the Einstein cross; Huchra et al. 1985). A simple calculation suggests that NGC 5532 is capable of forming an arc from a background galaxy at a redshift of about 0.4, if that galaxy lies close to the line of sight through the nucleus of NGC 5532, and it would be interesting to obtain an optical spectrum of the brightest region of the arc to check this interpretation. The arc is not detected in the WFPC2 or ACS *HST* images of the galaxy, presumably due to the higher stellar background in these images, so that optical observations might be challenging.

The mass distribution capable of lensing an extended object into an arc could also greatly amplify the brightness of a point object lying near the same line of sight. This could be an interpretation of the great over-brightness of the X-rays from the soft source discussed in Section 5.1, provided that this also lies at a significant
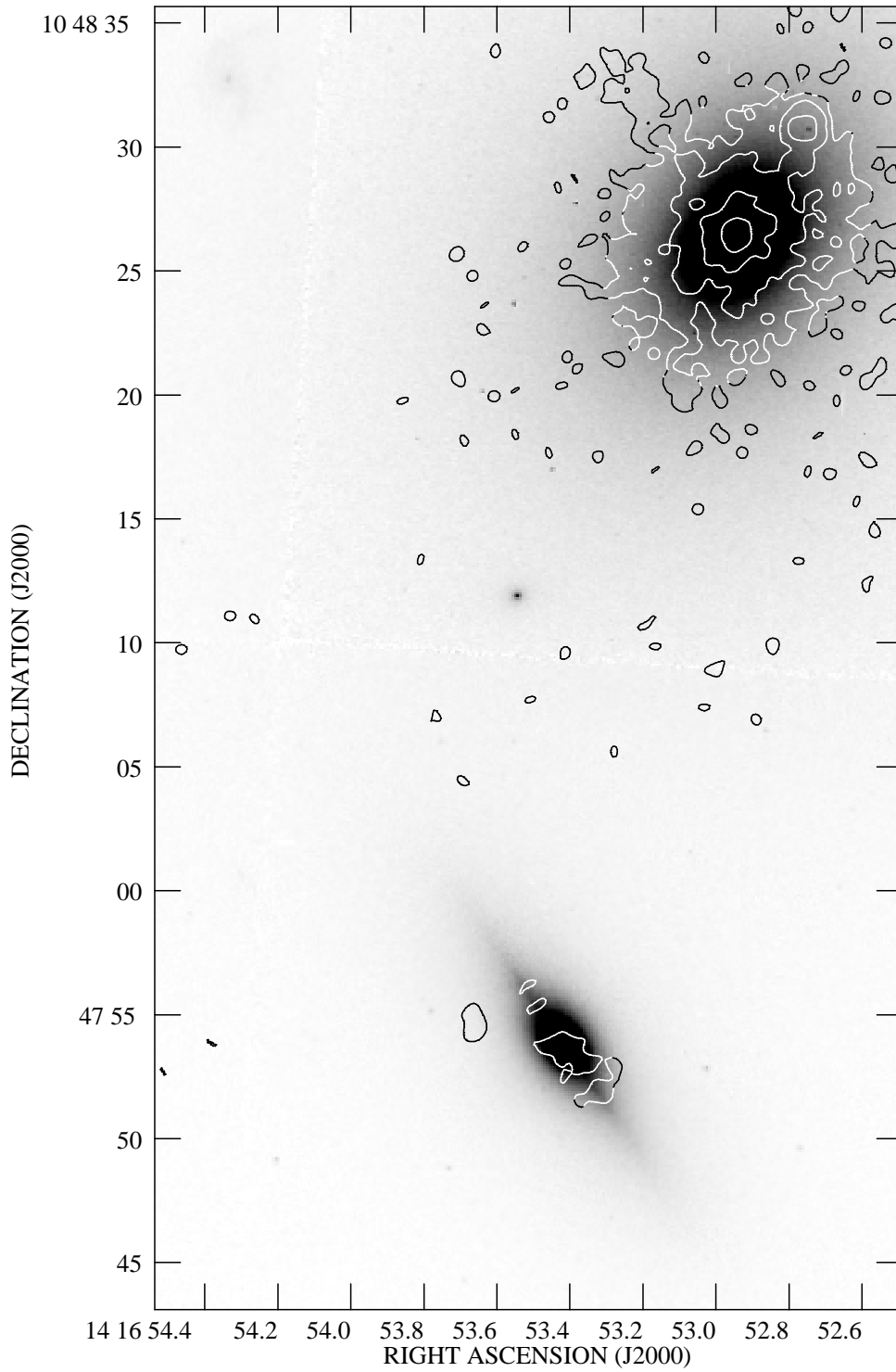
Figure 4. The X-ray emission detected by *Chandra* superposed on an archival *Hubble Space Telescope* WFPC2 image of the area around NGC 5532. The X-ray contours are from the smoothed X-ray image shown in Fig. 1; the lowest contour is at approximately 3σ above background (Hardcastle 2002). The *HST* image is the snapshot image in the F702W filter presented by Martel et al. (1999). The X-ray point source to the northwest of 3C 296 is close to a faint optical point source: the extended X-ray source to the south is associated with the spiral companion galaxy.
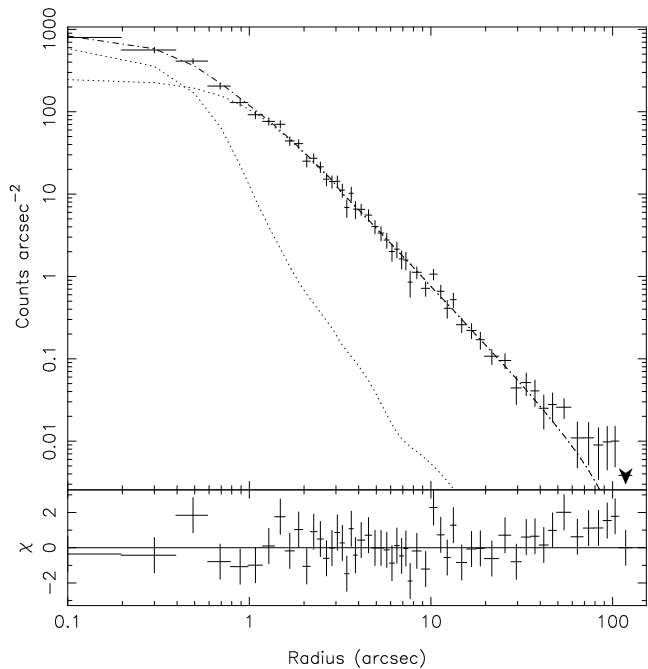
Figure 5. The radial profile of the extended emission centred on the nucleus of 3C 296, with the two components of the fitted model described in the text, their sum, and the residuals.

redshift. The arc and the soft source could then originate in the same group of galaxies at redshift ~ 0.4.

6 THE EXTENDED EMISSION

Spatially resolved emission is seen in the X-ray image of 3C 296 out to at least 30 arcsec from the X-ray nucleus, although most of the counts are on small angular scales. We used the same process as for 3C 31 (Hardcastle et al. 2002) to extract a radial profile from the 0.5–7.0 keV events dataset. The profile was centred on the nucleus, and excluded all detected point sources, as well as the jet region. It extended to 110 arcsec from the core, with background being taken between 110 and 130 arcsec; this ensures that all of the radial profile region falls on the S3 chip. Exposure correction was made using a map calculated at the peak energy of the dataset, 0.9 keV. We fitted the resulting profile (Fig. 5) with a model consisting of a point source (we use the PSF parametrization of Worrall et al. 2001) and a free β model. Unsurprisingly, a point-source model alone was an unacceptable fit to the data. A good fit was obtained ($\chi^2 = 48$ for 51 degrees of freedom) by adding a β model with $\beta = 0.56 \pm 0.01$, $\theta_c = 0.7^{+0.14}_{-0.10}$ arcsec (errors are 1σ for two interesting parameters). The unresolved core component contained 465 ± 40 counts in this model (consistent with the 530^{+240}_{-160} counts in the power-law spectral component), while the central normalization of the β model was 300 ± 60 counts arcsec^{-2}. There is little evidence in these fits for extended emission from the 3C 296 group on larger scales, although the positive residuals at 50–100 arcsec in Fig. 5 may give an indication of its presence. We do not attempt to characterize the large-scale extended emission, as it clearly makes only a small contribution, if any, to the radial profile on the S3 chip.

To determine the spectral properties of the extended emission, we used XSPEC to carry out fits of MEKAL models to annular regions centred on the galaxy (the regions used are listed in Table 1),

Table 1. Regions fitted with thermal models

Region (arcsec)	kT (keV)	Power-law luminosity (2–10 keV) (ergs s^{-1})	χ^2/d.o.f.
0–2.5	0.68 ± 0.02	N/A	71/55
2.5–5.0	$0.78^{+0.04}_{-0.04}$	$(1 \pm 1) \times 10^{40}$	20/13
5.0–12.5	$0.84^{+0.03}_{-0.05}$	$(3^{+0.5}_{-1}) \times 10^{40}$	18/14
12.5–30	0.82 ± 0.08	$(1.5 \pm 1) \times 10^{40}$	12/7

For the 0–2.5 arcsec region the power-law model was fixed to the parameters previously determined (Section 3).

excluding the nearby point source and jet emission regions. In the central region we included a power-law model with intrinsic absorption, as discussed in Section 3. Initially, we allowed both the temperature and the abundance to vary freely, while keeping the absorption column fixed at the Galactic value. We found that this produced poor fits in several annuli, notably the one between 5 and 12.5 arcsec: there were large residuals at high energies, though the fits were reasonable below 1 keV. We therefore fitted each annulus with a combination of a MEKAL model and a power law with no absorption in excess of Galactic and a fixed photon index of 1.0, which was intended to represent a contribution from X-ray binaries. This brought the fitting statistic to an acceptable level in all cases. The best-fitting abundance was high, with a joint fit to all four regions giving $Z = 1.4^{+0.9}_{-0.4}$ solar. As we regard such high metal abundances as a priori unlikely given our measurements from other sources and other work (e.g. Matsushita, Ohashi & Makishima 2000), we have fixed abundances to 0.5 in the fits tabulated in Table 1. As the Table shows, the luminosities of the best-fitting power-law components sum to a few $\times 10^{40}$ ergs s^{-1}, which is plausible for an elliptical galaxy with $M_B = -21.8$ (e.g. Matsumoto et al. 1997).

Apart from the lower best-fitting temperature in the central few arcsec, which we also observed in 3C 31, there is little evidence here for a temperature gradient: the temperatures beyond 2.5 arcsec are all consistent at the 1σ level with a value of 0.82 keV. An onion-skin deprojection similarly provides only marginal evidence for a temperature gradient. We do not yet know the temperature of the large-scale group emission, if any, around 3C 296 (a recent *XMM* observation will provide more information when it becomes available) but in the absence of other data we can model the atmosphere on the scales of interest as isothermal with a temperature $kT = 0.82$ keV beyond 2.5 arcsec. Assuming that there is no abundance gradient, it is then straightforward to determine the external pressure profile (Birkinshaw & Worrall 1993). Here we neglect the hard component in the spectrum which we have associated with X-ray binaries, since it contributes a small fraction of the count density on the sky. The central particle density of the β-model fit is then $(7\pm1)\times10^5$ m^{-3}, and the pressure and density as functions of radial distance are plotted in Fig. 6. (This assumes an abundance of 0.5 solar; if the abundance were as high as the best-fitting value, 1.4 solar, the densities and corresponding pressures would be reduced by a factor 1.5.) As we found for 3C 31, there is a steep pressure gradient associated with the region of the X-ray jet. The pressure gradient here is steeper (d log P/d log $R \sim 1.6$ rather than 1.0 as in 3C 31) because of the smaller core radius of the thermal material. The cooling time of the hot gas that provides the pressure gradient is small, only $\sim 10^7$ years in the centre (Fig. 7), so that (also as with 3C 31) this component should be transient in the absence of energy input from the jet or elsewhere. It seems that the association between a small-scale component of gas with a short cooling time
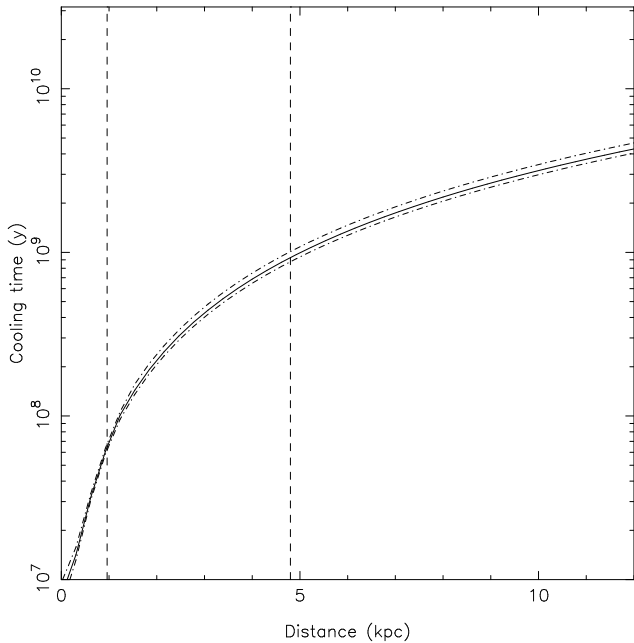
Figure 7. Cooling time as a function of radius in 3C 296. Lines and models as in Fig. 6.

and the jet may, as we suggested in the case of 3C 31, be a general requirement on jet deceleration models, and this again raises interesting questions about the relationship between the cooling gas and the energy supplied by the jet.

The minimum pressure in the jet on the assumption of a pure electron-positron plasma with a minimum electron Lorentz factor of 1, determined using the spectrum discussed in Section 4 and neglecting projection, is less than the external pressure for the length of the X-ray jet region (as was the case for 3C 31; Laing & Bridle 2002b), by factors of between about 10 and 1.5. This is not surprising, as there must be additional contributions to the internal pressure of the jet, and there is no compelling reason to expect the minimum-energy condition to be satisfied in this region.

7   SUMMARY AND CONCLUSION

Our *Chandra* observations have detected the nucleus and the jet of 3C 296 and have resolved the hot gas in the inner parts of the host galaxy. We have also detected the nearby galaxy NGC 5531, a bright nearby spiral galaxy, and a soft point source close to NGC 5532.

The non-thermal component of the X-ray core of 3C 296 has a higher best-fitting column density for intrinsic obscuration than is typical in twin-jet FRI sources, but we see neither the high column density nor the other X-ray features of an obscured active nucleus.

The X-ray jet of 3C 296 is towards the faint end of the observed range in X-ray to radio ratio for this type of jet, but the best-fitting spectral index and the available constraints on the overall SED of the jet, including a weak detection in the UV with the STIS instrument on *HST*, make us confident that this is another example of X-ray synchrotron emission from the inner jet of an FRI source. As with other sources of this kind, the X-ray emission is spatially closely associated with the region inferred from radio observations to be where jet deceleration is taking place.

The detection of a dense, small-scale thermal medium in the

centre of 3C 296's host galaxy is in agreement with observations of other FRIs (Worrall et al. 2001, 2003; Hardcastle et al. 2001, 2002; Donato et al. 2004) and with the predictions we made based on the 3C 31 data. A quantitative comparison between the X-ray data and a detailed model of the radio structure of the jet will be presented elsewhere.

REFERENCES

Allen, M.G., et al., 2002, ApJS, 139, 411
Birkinshaw, M., Laing, R.A., Peacock, J.A., 1981, MNRAS, 197, 253
Birkinshaw, M., Worrall, D.M., 1993, ApJ, 412, 568
Chiaberge, M., Macchetto, F.D., Sparks, W.B., Capetti, A., Allen, M.G., Martel, A.R., 2002, ApJ, 571, 247
Donato, D., Sambruna, R.M., Gliozzi, M., 2004, ApJ in press
Evans, D.A., Kraft, R.P., Worrall, D.M., Hardcastle, M.J., Jones, C., Forman, W.R., Murray, S.S., 2004, ApJ, 612, 786
Fabbiano, G., Miller, L., Trinchieri, G., Longair, M., Elvis, M., 1984, ApJ, 277, 115
Gliozzi, M., Sambruna, R.M., Brandt, W.N., 2003, A&A, 408, 949
Hardcastle, M.J., Alexander, P., Pooley, G.G., Riley, J.M., 1997, MNRAS, 288, L1
Hardcastle, M.J., Birkinshaw, M., Worrall, D.M., 2001, MNRAS, 326, 1499
Hardcastle, M.J., Worrall, D.M., 1999, MNRAS, 309, 969
Hardcastle, M.J., Worrall, D.M., Birkinshaw, M., Laing, R.A., Bridle, A.H., 2002, MNRAS, 334, 182
Hardcastle, M.J., Worrall, D.M., Kraft, R.P., Forman, W.R., Jones, C., Murray, S.S., 2003, ApJ, 593, 169
Huchra, J., Gorenstein, M., Kent, S., Shapiro, I., Smith, G., Horine, E., Perley, R., 1985, AJ, 90, 691
Laing, R.A., Bridle, A.H., 2002a, MNRAS, 336, 328
Laing, R.A., Bridle, A.H., 2002b, MNRAS, 336, 1161
Laing, R.A., Parma, P., de Ruiter H.R., Fanti, R., 1999, MNRAS, 306, 513
Leahy, J.P., Perley, R.A., 1991, AJ, 102, 537
Lynds, R., Petrosian, V., 1989, ApJ, 336, L1
Martel, A.R., et al., 1999, ApJS, 122, 81
Matsushita, K., Ohashi, T., Makishima, K., 2000, PASJ, 52, 685
Matsumoto, H., Koyama, K., Awaki, H., Tsuru, T., Loewenstein, M., Matsushita, K., 1997, ApJ, 482, 133
Miller, N.A., Owen, F.N., Burns, J.O., Ledlow, M.J., Voges, W., 1999, AJ, 118, 1988
Miller, N.A., Ledlow, M.J., Owen, F.N., Hill, J.M., 2002, AJ, 123, 3018
Mukai, K., Pence, W.D., Snowden, S.L., Kuntz, K.D., 2003, ApJ, 582, 184
Ueno, S., Koyama, K., Nishida, M., Yamauchi, S., Ward, M.J., 1994, ApJ, 431, L1
Worrall, D.M., Birkinshaw, M., Hardcastle, M.J., 2001, MNRAS, 326, L7
Worrall, D.M., Birkinshaw, M., Hardcastle, M.J., 2003, MNRAS, 343, L73
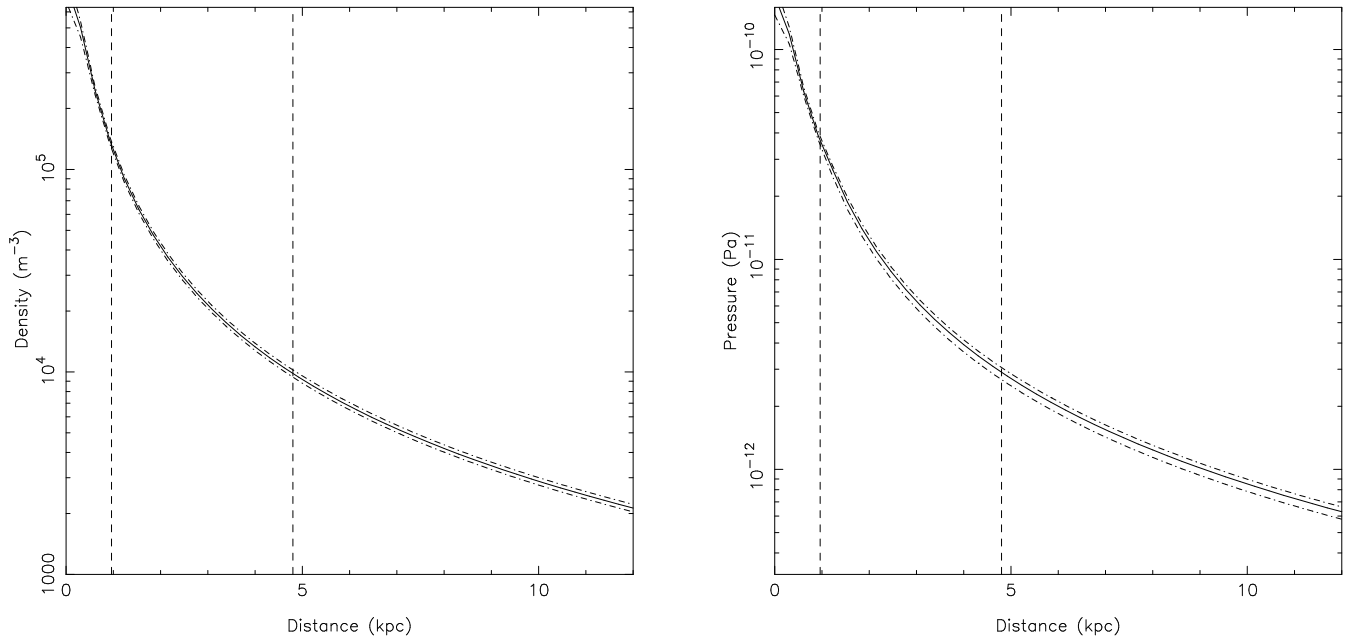Worrall, D.M., Birkinshaw, M., Hardcastle, M.J., Lawrence, C.R., 2001, MNRAS, 326, 1127

Figure 6. Proton density (left) and pressure (right) as a function of radius in 3C 296, based on the model described in the text. The solid black lines show the density and pressure derived from the best-fitting β models ($\beta = 0.56$, $r_c = 0.7$) and the fitted temperature. The surrounding dotted lines show the combined 1σ uncertainties due to the conversion between central normalization and density, the uncertainties on the β model fits and the uncertainty on temperature. The vertical dotted lines show the (projected) start and end of the X-ray jet. A linear temperature gradient between 0.6 and 0.82 ± 0.04 keV is assumed in the inner 2.5 arcsec.